Investigation of $Sm_{0.5}Sr_{0.5}CoO_{3-\delta}/Co_3O_4$ composite cathode for intermediate-temperature solid oxide fuel cells

Haizhou Zhang, Huanying Liu, You Cong, Weishen Yang *

State Key Laboratory of Catalysis, Dalian Institute of Chemical Physics, Chinese Academy of Sciences, Dalian 116023, China

ABSTRACT

The electrochemical properties of an $Sm_{0.5}Sr_{0.5}CoO_{3-\delta}/Co_3O_4$ (SSC/Co_3O_4) composite cathode were investigated as a function of the cathode-firing temperature, SSC/Co_3O_4 composition, oxygen partial pressure and CO_2 treatment. The results showed that the composite cathodes had an optimal microstructure at a firing temperature of about 1100 °C, while the optimum Co_3O_4 content in the composite cathode was about 40 wt.%. A single cell with this optimized C_{40}-1100 cathode exhibited a very low polarization resistance of 0.058 Ω cm^2, and yielded a maximum power density of 1092 mW cm^{-2} with humidified hydrogen fuel and air oxidant at 600 °C. The maximum power density reached 1452 mW cm^{-2} when pure oxygen was used as the oxidant for a cell with a C_{30}-1100 cathode operating at 600 °C due to the enhanced open-circuit voltage and accelerated oxygen surface-exchange rate. X-ray diffraction and thermogravimetric analyses, as well as the electrochemical properties of a CO_2-treated cathode, also implied promising applications of such highly efficient SSC/Co_3O_4 composite cathodes in single-chamber fuel cells with direct hydrocarbon fuels operating at temperatures below 500 °C.

© 2008 Elsevier B.V. All rights reserved.

1. Introduction

Solid oxide fuel cells (SOFCs) are one of the most promising fuel cell technologies for highly efficient and environmentally benign energy transformation, and they have attracted increasing attention in recent years [1–5]. However, due to the low ionic conductivity of yttria-stabilized zirconia (YSZ) and the low rate characteristics of $La_{1-x}Sr_xMnO_{3-\delta}$ (LSM) cathodes, conventional YSZ electrolyte-based fuel cells must be operated at high temperature (>800 °C) in order to obtain a considerable power output [6]. Degradation of the cell components, the high cost of fabrication and the poor stability associated with a high operating temperature, as well as their stringent material and processing requirements, prevent the commercial use of high-temperature SOFCs. In order to extend the range of possible materials, reduce the fabrication cost and improve the long-term stability of SOFCs, it appears inevitable that their operating temperature must be reduced to intermediate temperatures (500–700 °C). However, both the rapid increase in ohmic polarization and cathodic polarization result in a considerable decrease in cell performance if the operating temperature is reduced [7,8].

Decreasing the electrolyte thickness, adopting electrolyte materials with a higher ionic conductivity than YSZ, or a combination of these two approaches, will improve the cell performance to some extent through the subsequent decrease in ohmic resistance [9–11]. However, since the activation energy of cathodic polarization is higher than that of ohmic polarization, the ratio of cathodic resistance to electrolyte resistance increases from less than one to much more than one with a further decrease in operating temperature [12], so the cathodic polarization then becomes dominant in cell performance.

The electrochemical reduction of molecular oxygen to oxygen ions and the transfer of these ions from the bulk cathode to the electrolyte/cathode interface requires the cathode materials to have both oxygen-ion and electron conductivities. Thus, the oxygen-reduction reaction could take place at or near the triple phase boundaries (TPBs) of the cathode, the electrolyte, and the gas phase when an electronic conductor (such as Pt) is used as the cathode material. However, a considerable decrease in the cathode polarization resistance could be achieved if mixed electronic and ionic conductors (MIECs) are used as cathode materials, because they could extend the electrochemical active area from just the TPBs to the entire MIEC surface [13,14]. For example, the cathode polarization resistances of $La_{0.6}Sr_{0.4}Co_{0.2}Fe_{0.8}O_{3-\delta}$ (LSCF)–$Ce_{0.9}Gd_{0.1}O_{2-\delta}$ (GDC) on a GDC electrolyte and $Sm_{0.5}Sr_{0.5}CoO_{3-\delta}$ (SSC)–$Sm_{0.2}Ce_{0.8}O_{2-\delta}$ (SDC) on an SDC electrolyte are only ∼0.2 Ω cm^2 and less than 0.18 Ω cm^2 at

* Corresponding author. Tel.: +86 41184379073; fax: +86 41184694447.
E-mail address: yangws@dicp.ac.cn (W. Yang).
URL: http://www.yanggroup.dicp.ac.cn (W. Yang).

600 °C [12,15], respectively, but the cathode polarization resistance of $La_{0.8}Sr_{0.2}MnO_{3-\delta}$ (LSM)–$Ce_{0.8}Gd_{0.2}O_{2-\delta}$ (GDC) on a GDC electrolyte is as high as 4.44 Ω cm^2 at 600 °C [8]. Although MIEC cathode material exhibits a much lower polarization resistance and yields considerable improvements in cell performance at lower temperature, e.g. a maximum power density of 167 or 231 mW cm^{-2} at 500 °C [16,17], the performance is still far from the value forecasted by Steele, i.e. a maximum power density of ~400 mW cm^{-2} at 500 °C with a 25 μm thin-film SDC electrolyte [18]. This expected value was finally achieved when the excellent oxygen-permeable membrane material, $Ba_{0.5}Sr_{0.5}Co_{0.8}Fe_{0.2}O_{3-\delta}$ (BSCF) [19], was used as cathode material. BSCF exhibits very low polarization resistance due to its high oxygen diffusion coefficient and yields maximum power densities as high as 402 mW cm^{-2} at 500 °C [20]. However, the easy formation of barium carbonates for BSCF with CO_2 greatly limits its application as a cathode material [21,22]. Therefore, highly efficient, stable and chemical-compatible cathode materials are still urgently needed. In our previous work, Co_3O_4 was introduced into perovskite $Ln_xSr_{1-x}CoO_{3-\delta}$ (Ln = La, Sm, Gd) cathode materials to improve their oxygen-reduction ability, and very exciting results were achieved [23]. In this paper, more detailed investigations will be presented on how the electrochemical properties of $Sm_{0.5}Sr_{0.5}CoO_{3-\delta}/Co_3O_4$ composite cathodes depend on the cathode firing temperatures, the relative proportions of SSC and Co_3O_4, and the effects of oxygen partial pressure and CO_2 treatment.

2. Experimental

2.1. Powder preparation

SDC, GDC, SSC and Co_3O_4 powders were synthesized by a citrate and EDTA process [24]. Stoichiometric amounts of metal nitrate solutions were introduced into a beaker and equal molar proportions of citrate and EDTA with respect to total metal ions were added to the mixed solution, to which an appropriate amount of ammonium nitrate was specially added for the preparation of a foamy powder of SDC. After the pH value was adjusted close to 8 with ammonia, the solution was heated and evaporated on a hot plate at 80 °C. The resulting viscous gel was first calcined at ~500 °C to remove organic compounds, and then calcined for 2 h under stagnant air at 700–950 °C.

2.2. Fuel cell fabrication

The anode-supported thin-film electrolyte was assembled using the co-pressing method [10]. Equal weights of GDC and commercial NiO powder were first mixed, ground with alcohol and dried, then the dried mixed powder was pressed at 100 MPa to form a substrate. Subsequently, a foamy powder of SDC was distributed uniformly and pressed onto the substrate at 200 MPa. The green bilayer assembly, which was ~22 mm in diameter and 1 mm thick, was fired at 1450 °C for 4 h in an air atmosphere, resulting in an SDC electrolyte film about 25 μm thick by controlling the quantity of SDC foamy powder. To narrow the difference of thermal-expansion coefficients between the electrolyte and cathode, a paste of SDC/SSC (70:30 wt.%) mixture dispersed in terpineol was first applied to the electrolyte surface as an interlayer by the doctor blade process. Then a paste containing different amounts of Co_3O_4 (0–50 wt.%) and SSC was similarly applied to the interlayer as the cathode. The cell was subsequently fired for 2 h at 1050–1150 °C in air, the final cathode was about 100 μm thick, with an ~30 μm interlayer and ~0.33 cm^2 effective cathode area. The cathodes were named according to their composition and firing temperature; for exam-
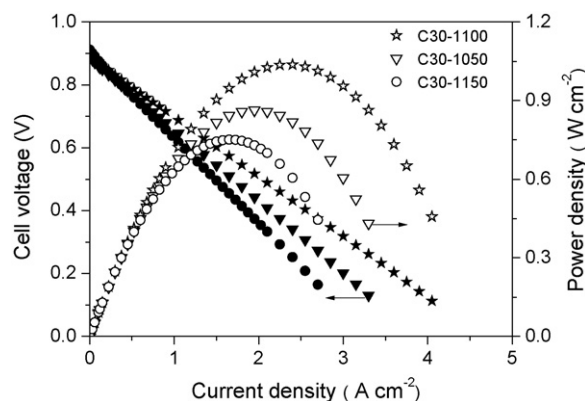

Fig. 1. Voltages and power densities as a function of current density for cells with C_{30} cathodes fired at different temperatures. Test conditions: 3 vol.% H_2O-humidified H_2 at 100 ml min^{-1} for the anode and air at 400 ml min^{-1} for the cathode at 600 °C.

ple, C_{30}-1100 denoted an SSC/Co_3O_4 cathode consisting of 30 wt.% Co_3O_4 fired at 1100 °C for 2 h.

2.3. Fuel cell characterization

The fuel cells were tested using a two-electrode configuration under ambient pressure, in which humidified hydrogen (3 vol.% H_2O) was fed as fuel and air as oxidant. Current–voltage (*I–V*) characteristics of the cells were measured at various current densities by changing the external load. The impedance of single cells was measured under open-circuit conditions from 10 mHz to 10^5 Hz using an EG&G lock-in amplifier (model 5210) in combination with an EG&G potentiostat/galvanostat (model 263A). The morphologies of the tested cathodes were observed using an FEI Quanta 200F scanning electron microscope.

2.4. X-ray diffraction and thermogravimetric analyses

XRD analysis was performed on a Rigaku D/Max-2500 diffractometer using Cu K_α radiation (λ = 1.54108 Å) at 40 kV and 250 mA, whereas TG analysis was carried out on a Perkin-Elmer Pyris Diamond TG/DTA analyzer with a heating rate of 10 °C min^{-1} under 100 ml min^{-1} 20% CO_2/air for SSC and 100 ml min^{-1} 100% CO_2 for Co_3O_4, respectively.
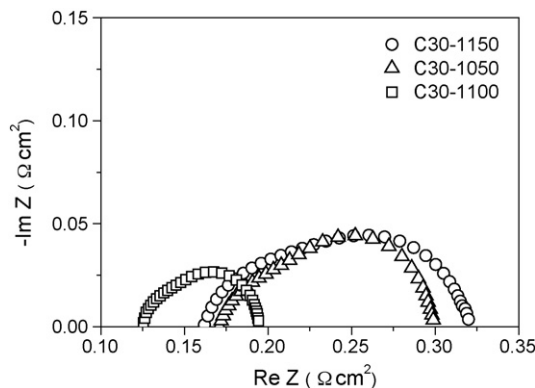

Fig. 2. Impedance spectra for cells with C_{30} cathodes fired at different temperatures. Test conditions: two-electrode configuration under open-circuit voltage at 600 °C.

3. Results and discussion

3.1. Effects of cathode firing temperature

It is generally considered that the overall cathode process is a heterogeneous chemical reaction consisting of several elemental steps, such as gas diffusion and adsorption of O_2, surface diffusion and incorporation of adsorbed oxygen, bulk diffusion and charge transfer of oxygen ions, etc. [25]. One or more limiting steps exist that control the total reaction rate of the cathode process and determine the cathode performance. For a given cathode material, the cathode reaction rate is a function of microstructural variables, such as the particle size, the length of the TPBs, the porosity and the bonding state between the cathode and the electrolyte [26]. These physical parameters can be optimized by adopting an appropriate firing temperature.

The performance and polarization resistance of cells with a C_{30} cathode fired at different temperatures were investigated at 500, 550 and 600 °C. The dependence of the cell voltages and power densities on current densities for different cathodes at 600 °C, as well as the impedance spectra, are shown in Figs. 1 and 2, respectively, and all the experimental data, including the maximum power density (P_{max}), the ohmic resistance (R_s) and the polarization resistance (R_p), are summarized in Table 1. Although R_p presents the sum of the cathode and anode polarizations in a two-probe configuration, it can be mainly attributed to the cathode polarization resistance due to the negligible anode polarization resistance in fuel cells with an Ni-based anode and hydrogen fuel [10]. It is found from Table 1 that the cell with a C_{30}-1100 cathode showed much lower polarization resistance than cells with C_{30}-1050 and C_{30}-1150 cathodes, thus displaying the best cell performance. For example, the polarization resistance was as low as 0.069 Ω cm^2, while the maximum power density reached 1037 mW cm^{-2} for the cell with a C_{30}-1100 cathode at 600 °C. For the cells with C_{30}-1050 and C_{30}-1150 cathodes, the polarization resistances increased to 0.127 and 0.158 Ω cm^2, and this resulted in the maximum power densities decreasing to 863 and 752 mW cm^{-2}, respectively.

Fig. 3 shows typical cross-sectional SEM images of C_{30} cathodes fired at 1050, 1100 and 1150 °C for 2 h, respectively. The grain size of the C_{30}-1100 cathode ($\sim$1 μm) was slightly larger than that of the C_{30}-1050 cathode (<1 μm), but much smaller than that of the C_{30}-1150 cathode ($\sim$4 μm). For the C_{30}-1150 cathode, its low porosity and specific area, due to the larger grain size, limited the gas transportation and decreased the number of reactive sites in the bulk cathode, consequently yielding the large polarization resistances shown in Fig. 2. In contrast, the C_{30}-1050 cathode also exhibited a lower cell performance than that of the C_{30}-1100 cathode in spite of its smaller grain size. As shown in Fig. 2, such performance degradation may result from high charge-transfer resistance and high ohmic resistance, which are associated with the poor state of bonding between the electrolyte and cathode under a relatively lower firing temperature.

3.2. Effect of Co_3O_4 content

Fig. 4 shows the cell performance for SSC/Co_3O_4 cathodes with different contents of Co_3O_4 (0–50 wt.%). The results clearly demonstrate that the introduction of Co_3O_4 into an SSC cathode can greatly improve the cell performance, e.g. for a C_{10}-1100 cathode, the maximum power densities reached 245 mW cm^{-2} at 500 °C and 787 mW cm^{-2} at 600 °C, whereas the corresponding values for an SSC cathode were 201 and 618 mW cm^{-2}. A further increase in Co_3O_4 content could lead to more improvements of cell performance up to a Co_3O_4 content of 40 wt.%, for which the maximum power densities were as high as 412 mW cm^{-2} at 500 °C and
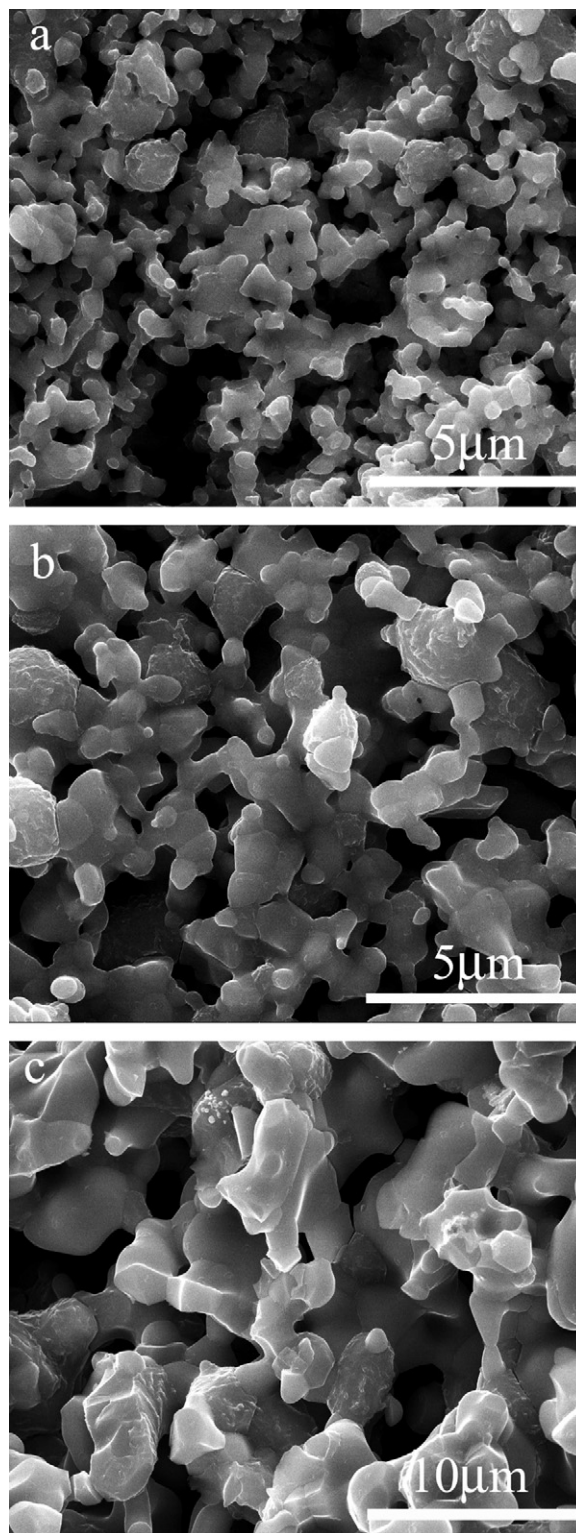

Fig. 3. Cross-sectional SEM images of SSC/Co_3O_4 (70:30 wt.%) composite cathodes fired at (a) 1050 °C, (b) 1100 °C and (c) 1150 °C.

1092 mW cm^{-2} at 600 °C, respectively. Although the performance of a C_{50}-1100 cathode was inferior to that of C_{40}-1100 and C_{30}-1100 cathodes, its maximum power densities (343 mW cm^{-2} at 500 °C and 958 mW cm^{-2} at 600 °C) were still higher than that of a C_{20}-1100 cathode (301 mW cm^{-2} at 500 °C and 904 mW cm^{-2} at 600 °C).

Table 1
Electrochemical properties of cells with a C_{30} cathode fired at different temperatures and operating at 500, 550 and 600 °C

Cathode	500 °C			550 °C			600 °C		
	P_{max} (mW cm^{-2})	R_s (Ω cm^2)	R_p (Ω cm^2)	P_{max} (mW cm^{-2})	R_s (Ω cm^2)	R_p (Ω cm^2)	P_{max} (mW cm^{-2})	R_s (Ω cm^2)	R_p (Ω cm^2)
C_{30}-1050	260	0.483	0.953	523	0.265	0.238	863	0.171	0.127
C_{30}-1100	381	0.354	0.436	622	0.187	0.173	1037	0.125	0.069
C_{30}-1150	233	0.412	1.231	481	0.223	0.334	752	0.162	0.158

P_{max}: maximum power density, R_s: cell ohmic resistance, R_p: electrode polarization resistance.

Fig. 5 shows the impedance spectra for cells with SSC/Co$_3$O$_4$ composite cathodes with different contents of Co$_3$O$_4$. As a good MIEC, SSC exhibited a moderate polarization resistance of 0.204 Ω cm^2 at 600 °C, but this value rapidly increased to 1.512 Ω cm^2 at 500 °C. Similarly to the cell performance, the addi-

tion of Co$_3$O$_4$ caused an evident decrease in polarization resistance, e.g. 1.023, 0.321 and 0.143 Ω cm^2 at 500, 550 and 600 °C for a C$_{10}$-1100 cathode. When the Co$_3$O$_4$ content increased up to 40 wt.%, the polarization resistance reached a minimum in this range of experiments, i.e. 0.417 Ω cm^2 at 500 °C, 0.154 Ω cm^2 at 550 °C and 0.058 Ω cm^2 at 600 °C. A subsequent further increase in Co$_3$O$_4$ content led to an obvious increase in polarization resistance; for example, a C$_{50}$-1100 cathode displayed polarization resistances of 0.653, 0.198 and 0.085 Ω cm^2 at 500, 550 and 600 °C, respectively. Meanwhile, due to the electronic conductivity of the doped ceria electrolyte and the different cathode exchange-current densities associated with the catalytic activity of the cathode material, the internal short-circuit current density of the electrolyte increased when the cathode catalytic activity improved and the cell operation temperature increased, thus resulting in a decrease in cell ohmic resistance as shown in Fig. 5(a).

In general, the electrochemical impedance spectra (EIS) are acquired under open-circuit conditions and show the equilibrium characteristics of the electrodes, whereas the overpotential over
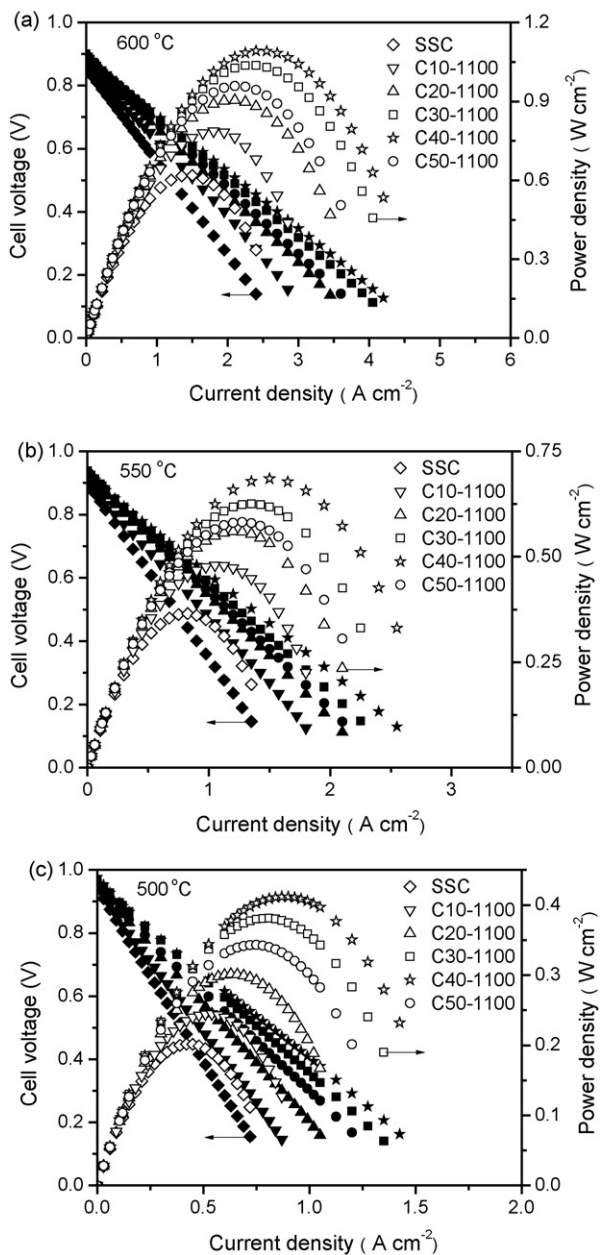

Fig. 4. Voltages and power densities as a function of current density for cells with SSC/Co$_3$O$_4$ composite cathodes with different Co$_3$O$_4$ contents. Test conditions: 3 vol.% H$_2$O-humidified H$_2$ at 100 ml min^{-1} for the anode and air at 400 ml min^{-1} for the cathode at (a) 600 °C, (b) 550 °C and (c) 500 °C.
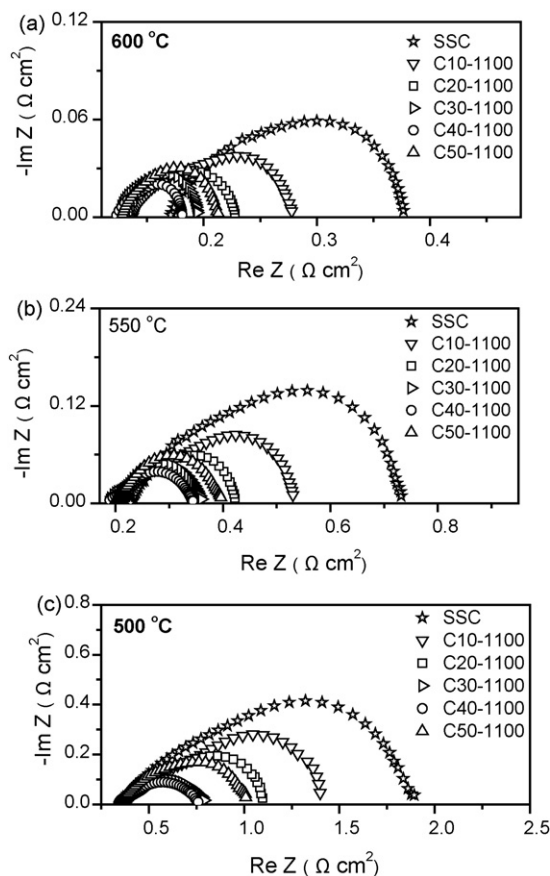

Fig. 5. Impedance spectra for cells with SSC/Co$_3$O$_4$ composite cathodes having different Co$_3$O$_4$ contents. Test conditions: two-electrode configuration under open-circuit voltage at (a) 600 °C, (b) 550 °C and (c) 500 °C.
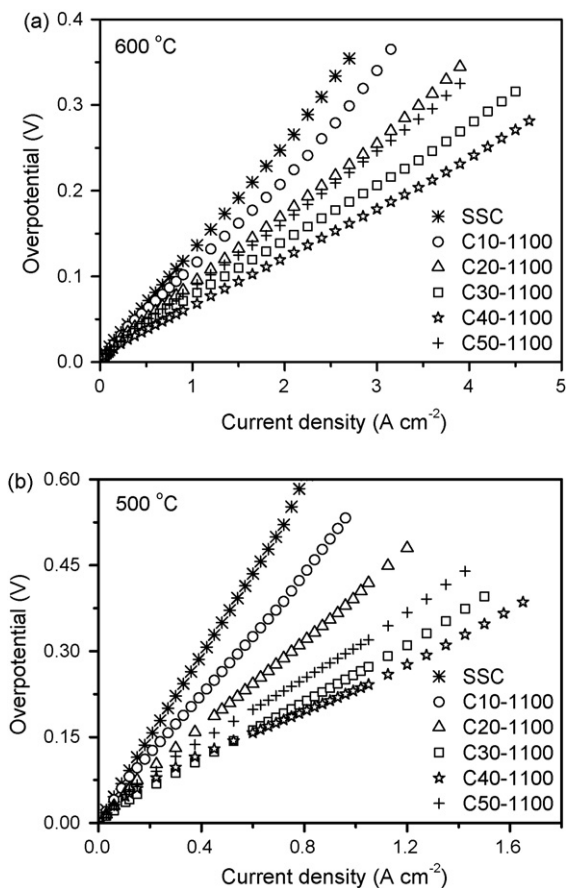
Fig. 6. Electrode overpotentials as a function of current density for cells with SSC/Co₃O₄ composite cathodes having different Co₃O₄ contents obtained at (a) 600 °C and (b) 500 °C.

the electrodes reveals their non-equilibrium characteristics under cell discharge. Since there are no obvious changes in the ohmic resistance (R_s) of a cell whether it is discharging or not, the total overpotential (the sum of the anode and cathode overpotentials) η_T can be acquired from the following equation:

$$\eta_T = V_{OC} - V - IR_s$$

where the ohmic resistance R_s represents the intercept of the impedance spectrum with the real axis at high frequency, V_{OC} is the open-circuit voltage, and I and V are the discharge current density and corresponding terminal voltage of the cell, respectively. Unlike the anode polarization resistance, which can be negligible under equilibrium, the anode overpotential can contribute partially to the total electrode overpotential under cell operation conditions. Therefore, it is difficult to distinguish the cathode overpotential from the total overpotential in a two-electrode configuration fuel cell. Due to the identical anode and electrolyte assemblies (fabricated in batch processes under the same conditions) used in these experiments, there is no doubt that any change in the total overpotential among the cells can only result from the differences of the cathodes. Fig. 6 shows electrode overpotentials for cells with SSC/Co₃O₄ cathodes with different contents of Co₃O₄. The results clearly indicate that the overpotentials (i.e., the cathode overpotentials) decreased as the Co₃O₄ content increased up to 40 wt.%, and further increase in Co₃O₄ content made the overpotentials increase again. For example, the overpotential was 310 mV for an SSC cathode and obviously decreased to 241 mV for a C₁₀-1100 cathode if the cells were operated at 2.4 A cm⁻² working current density at
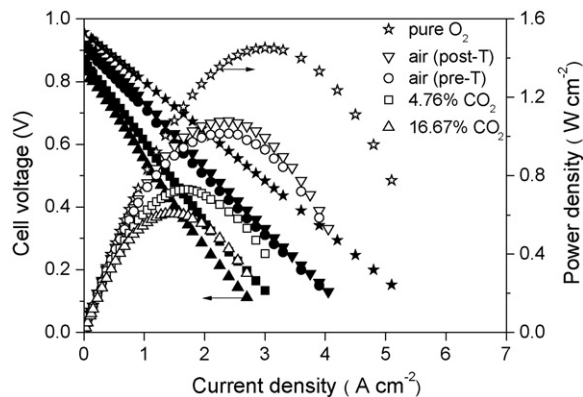

Fig. 7. Voltages and power densities as a function of current density for a cell with a C₃₀-1100 cathode under different concentrations of CO₂ and oxygen partial pressures. Test conditions: 3 vol.% H₂O-humidified H₂ at 100 ml min⁻¹ for the anode and different oxidants for the cathode at 600 °C.

600 °C. At same time, the overpotential gradually decreased to 193 and 158 mV for C₂₀-1100 and C₃₀-1100 cathodes, respectively, and reached the minimum value of 136 mV for C₄₀-1100. However, the overpotential began to increase to 184 mV for a C₅₀-1100 cathode.

3.3. Effect of O₂ partial pressure and CO₂ treatment

The effects of oxygen partial pressure and CO₂ treatment on cathode performance, including the cell performance and polarization resistance, were examined on another cell with a C₃₀-1100 cathode operating at 600 °C, and the results are shown in Figs. 7 and 8. The maximum power density reached 1015 mW cm⁻² with a total electrode polarization resistance of 0.065 Ω cm² when the cell was operated with air as oxidant. This indicated good reproducibility of cell performance compared with the C₃₀-1100 cathode described in Section 3.1.

After the oxidant gas line was switched from 400 ml min⁻¹ air to 80 ml min⁻¹ pure oxygen, the open-circuit voltage rapidly increased by ~50 mV from 0.906 to 0.958 V, which was far more than the increase expected from the Nernst equation (29.3 mV, from 1.1358 to 1.1651 V). This meant that the higher oxygen pressure in the cathode chamber had the beneficial effect of restraining the reduction of Ce⁴⁺ to Ce³⁺ within the doped ceria electrolyte, decreasing the fraction of electronic conductivity and increasing the open-circuit voltage of the cell. Due to this enhanced open-circuit voltage and the greatly increased number of active reaction
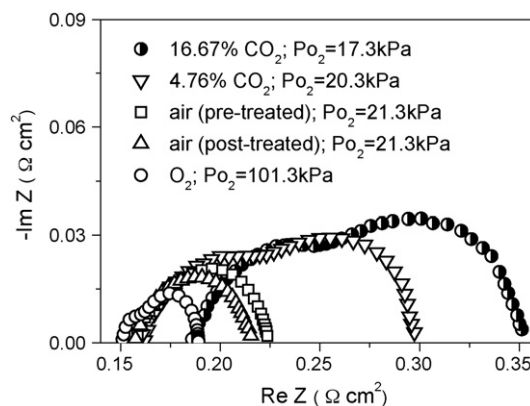

Fig. 8. Impedance spectra for a cell with a C₃₀-1100 cathode under different concentrations of CO₂ and oxygen partial pressures. Test conditions: two-electrode configuration under open-circuit voltage at 600 °C.

sites by exclusion of the competitive absorption of N_2, the maximum power density reached 1452 mW cm^{-2}, an ~40% increase in magnitude compared with air oxidant at 600 °C. In addition, the total electrode polarization resistance decreased to 0.038 Ω cm^2, a similar ~40% decrease in magnitude.

As a moderately active cathode material, SSC has been successfully utilized as the cathode in a single-chamber fuel cell with direct hydrocarbon fuels [27]. The much higher activity of an SSC/Co$_3$O$_4$ composite cathode than that of an SSC cathode implies more promising applications of composite cathodes in such fields. In view of the high concentration of CO_2 in a single-chamber fuel cell with direct hydrocarbon fuels, it was necessary to study the effect of CO_2 on the cathode performance. The results in Fig. 7 show that the maximum power density sharply decreased from 1015 to 730 mW cm^{-2} with the polarization resistance increasing from 0.065 to 0.136 Ω cm^2 (see Fig. 8) when the CO_2 concentration was 4.76%. As the CO_2 concentration continued increasing to 16.67%, the maximum power density slightly decreased to 608 mW cm^{-2} with the polarization resistance slightly increasing to 0.165 Ω cm^2. However, the cell performance could rapidly recover, and the maximum power density reached 1078 mW cm^{-2} again when the CO_2 was shut off and the oxidant gas line was switched to air, as shown in Fig. 7.

The XRD analysis results for SSC treated under different atmospheres are shown in Fig. 9. Compared with a fresh SSC sample, the XRD pattern for sample b indicates that some $SrCO_3$ (JCPDS 05-0418) and Co_3O_4 (JCPDS 43-1003) were formed when the SSC sample was exposed to a 25% CO_2 atmosphere for 50 h at 600 °C. The XRD pattern for sample c demonstrates that $SrCO_3$ and Co_3O_4 in sample b preferentially reacted with each other to form $SrCoO_{3-\delta}$ (JCPDS 49-0692) when sample b was exposed to an air atmosphere at 650 °C. The TG analysis of SSC and Co_3O_4 under a CO_2 atmosphere is shown in Fig. 10. It was found that SSC began to absorb CO_2 at 500 °C, with the weight of the sample continuously increasing due to the formation of $SrCO_3$ and Co_3O_4, whereas the formation rate of $SrCoO_{3-\delta}$ and CO_2 surpassed the formation rate of $SrCO_3$ and Co_3O_4 at ~800 °C, and resulted in the sample weight continuously decreasing. However, Co_3O_4 had no weight change even in the presence of pure CO_2 until it was converted into CoO at ~950 °C.

The results of the TG and XRD analyses demonstrate that some $SrCO_3$ and Co_3O_4 appeared on the surface of an SSC cathode when an SSC/Co$_3$O$_4$ composite cathode was exposed to a CO_2 atmosphere at 600 °C. It was the selective adsorption of CO_2 and the formation of carbonate that made the cell performance sharply decrease at low CO_2 concentrations. When the oxidant was switched back to
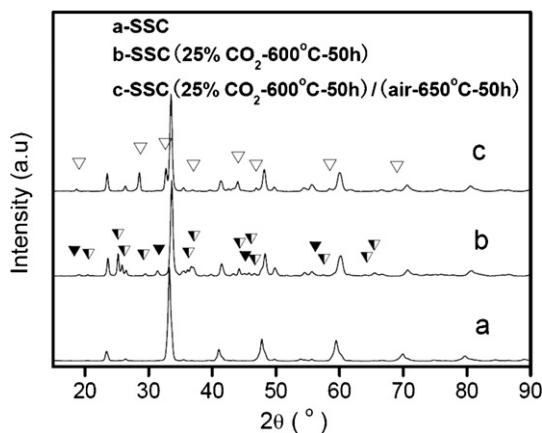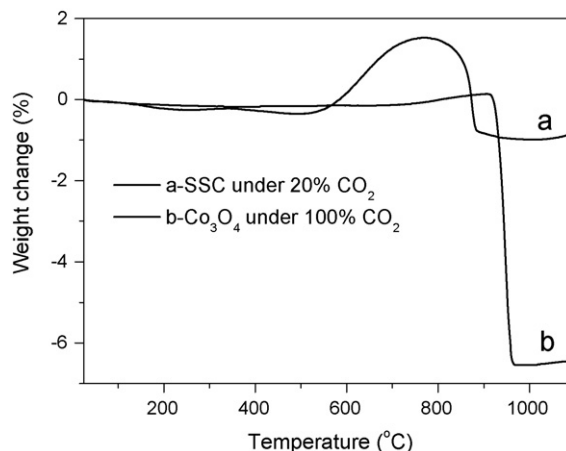

Fig. 10. TG analysis for SSC under 20% CO_2/air atmosphere and for Co_3O_4 in pure CO_2.

air, $SrCO_3$ and Co_3O_4 may react and be converted into $SrCoO_{3-\delta}$ at a cell operating temperature of 600 °C. The higher oxygen-vacancy concentration of $SrCoO_{3-\delta}$ than that of $Sm_{0.5}Sr_{0.5}CoO_{3-\delta}$ helps to increase the oxygen-ion conductivity of the cathode electrocatalyst. Provided that the cell operation temperature was not high enough for the formation of $SrCoO_{3-\delta}$, the existence of Co_3O_4 was also beneficial for improving the oxygen surface-exchange coefficient of the cathode material. Either the increase in oxygen-ion conductivity or the enhancement of the surface-exchange coefficient could accelerate the oxygen reduction rate in the overall cathode process, and consequently yielded some improvement in cell performance, as shown in Fig. 7.

4. Conclusions

The electrochemical properties of SSC/Co$_3$O$_4$ composite cathodes were investigated under various conditions. The dependence of the cathode performance on the firing temperature of the cathode indicated that at 1100 °C the composite cathodes acquired an optimized microstructure, which had good bonding between the cathode and electrolyte, relatively high porosity and high specific area. Unlike traditional composite cathodes, the performance of SSC/Co$_3$O$_4$ was not confined by the percolation limit, in which all the Co_3O_4 could take full effect until its content increased up to 40 wt.% due to the MIEC characteristic of SSC. By replacing the air oxidant with pure oxygen, the enhancement of the open-circuit voltage and the improvement of the oxygen surface-exchange rate resulted in ~40% increase in cell performance. The XRD and TG analyses revealed that a low CO_2 concentration in the oxidant could incur permanent effects on the SSC/Co$_3$O$_4$ composite cathode only if the cell operation temperature was above 500 °C.

Fig. 9. XRD analysis for (a) fresh SSC, (b) SSC treated with 25% CO_2 and air mixture at 600 °C for 50 h, and (c) sample b treated with air atmosphere at 600 °C for 50 h. (▼) Co_3O_4, (K) $SrCO_3$, (×) $SrCoO_{3-\delta}$.

References

[1] K. Huang, J. Wan, J.B. Goodenaugh, J. Electrochem. Soc. 148 (7) (2001) A788–A794.
[2] N.T. Harta, N.P. Brandon, M.J. Daya, N. Lapeña-Rey, J. Power Sources 106 (2002) 42–50.
[3] S.B. Adler, J.A. Lane, B.C.H. Steele, J. Electrochem. Soc. 143 (1996) 3554–3564.

[4] M. Mamak, N. Coombs, G. Ozin, J. Am. Chem. Soc. 122 (2000) 8932–8939.
[5] M. Juhl, S. Primdahl, C. Manon, M. Mogensen, J. Power Sources 61 (1996) 173–181.
[6] S. Jiang, Solid State Ionics 146 (2002) 1–22.
[7] S. Zha, A. Moore, H. Abernathy, M. Liu, J. Electrochem. Soc. 151 (8) (2004) A1128–A1133.
[8] E.P. Murray, S.A. Barnett, Solid State Ionics 143 (2001) 265–273.
[9] S. de Souza, S.J. Visco, L.C. de Jonghe, Solid State Ionics 98 (1997) 57–61.
[10] C. Xia, M. Liu, Solid State Ionics 144 (2001) 249–255.
[11] X. Zhang, S. Ohara, R. Maric, K. Mukai, T. Fukui, H. Yoshida, M. Nishimura, T. Inagaki, K. Miura, J. Power Sources 83 (1999) 170–177.
[12] C. Xia, F. Chen, M. Liu, Electrochem. Solid-State Lett. 4 (5) (2001) A52–A54.
[13] S.B. Adler, Solid State Ionics 111 (1998) 125–134.
[14] M. Koyama, C.J. Wen, T. Masuyama, J. Otomo, H. Fukunaga, K. Yamada, K. Eguchi, H. Takahashi, J. Electrochem. Soc. 148 (7) (2001) A795–A801.
[15] V. Dusastre, J.A. Kilner, Solid State Ionics 126 (1999) 163–174.
[16] Y. Leng, S. Chan, S. Jiang, K.A. Khor, Solid State Ionics 170 (2004) 9–15.
[17] C. Xia, M. Liu, Adv. Mater. 14 (2002) 521–523.
[18] B.C.H. Steele, Solid State Ionics 129 (2000) 95–110.
[19] Z.P. Shao, W.S. Yang, Y. Cong, G.X. Xiong, J. Membr. Sci. 172 (1–2) (2000) 177–188.
[20] Z. Shao, S.M. Haile, Nature 431 (2004) 170–173.
[21] A. Yan, M. Cheng, Y. Dong, W. Yang, V. Maragou, S. Song, P. Tsiakaras, Appl. Catal. B: Environ. 66 (2006) 64–71.
[22] A. Yan, V. Maragou, A. Arico, M. Cheng, P. Tsiakaras, Appl. Catal. B: Environ. 76 (3–4) (2007) 320–327.
[23] H. Zhang, W. Yang, Chem. Commun. 41 (2007) 4215–4217.
[24] X. Zhu, Y. Cong, W. Yang, J. Membr. Sci. 283 (2006) 158–163.
[25] T. Horita, K. Yamaji, N. Sakai, H. Yokokawa, A. Weber, E. vers-Tiffee, J. Electrochem. Soc. 148 (5) (2001) A456–A462.
[26] T.J. Armstrong, A.V. Virkar, J. Electrochem. Soc. 149 (12) (2002) A1565–A1571.
[27] T. Hibino, A. Hashimoto, T. Inoue, J. Tokuno, S. Yoshida, M. Sano, Science 288 (2000) 2031–2033.